AIMS Mathematics, 10(11): 26823–26843.
DOI:10.3934/math.20251179
Received: 16 August 2025
Revised: 27 October 2025
Accepted: 11 November 2025
Published: 19 November 2025

https://www.aimspress.com/journal/Math

Research article

Sensitivity, bifurcation behavior, stability and new traveling wave solutions for the stochastic Nizhnik-Novikov-Veselov system

Hafiz M. A. Siddiqui[1], Lotfi Jlali[2], A. Nazir[1], Syed T. R. Rizvi[1], Atef F. Hashem[2] and Aly R. Seadawy[3,*]

[1] Department of Mathematics, COMSATS University Islamabad , Lahore Campus, Lahore Pakistan

[2] Department of Mathematics and Statistics, College of Science, Imam Mohammad Ibn Saud Islamic University (IMSIU), Riyadh 11566, Saudi Arabia

[3] Mathematics Department, Faculty of Science, Taibah University, Al-Madinah Al-Munawarah 41411, Saudi Arabia

* **Correspondence:** Email: aabdelalim@taibahu.edu.sa.

Abstract: Nonlinear stochastic models play a crucial role in describing complex wave phenomena in multidimensional physical systems. Motivated by this, we investigated the Stochastic Nizhnik-Novikov-Veselov (SNNV) equation to explore its solitary wave dynamics, chaotic behavior, bifurcation structures, sensitivity, and stability characteristics. We used the extended modified auxiliary equation mapping (EMAEM) method, an enhanced analytical framework with greater flexibility and broader solution structures versus conventional methods. With this approach, we derived new families of exact solitary wave solutions, including single, dark, and bright singular solitons. The proposed methods explain dynamical characteristics that were previously unexplored for the SNNV equation. The stochastic model will be converted into a dynamical system using the Galilean transformation. This approach enables exploration of its dynamical behavior via stochastic processes. We used Poincaré maps, phase portraits, and time-series trajectory simulations to establish its strong stochastic behavior, including chaotic behavior. To show that these methods are dynamically stable, we conducted a stability analysis using the Hamiltonian system framework. The proposed study will significantly advance the dynamic interpretation of chaos in the SNNV equation and establish the superiority of EMAEM approach for wave structure formation.

Keywords: stochastic Nizhnik-Novikov-Veselov (SNNV) system; exact solutions; integrability
Mathematics Subject Classification: 35B10, 35C07, 35C08, 35Q35

1. Introduction

Nonlinear partial differential equations (NLPDEs) are used in many scientific fields and require trustworthy methods for modeling the underlying physical processes. Selecting the suitable PDE analysis and result interpretation procedures is essential. Numerous effective strategies have been developed, as every PDE presents unique challenges, despite the fact that there is no universal technique that works for all PDEs. Various famous methods include tanh expansion [1], modified extended tanh expansion [2], Adomian decomposition [3], Bäcklund transformation [4], Painlev*é* expansion [5], fractional homotopy analysis [6], Kudryashov's technique [7, 8], and the exponential rational function method [9]. Some other pertinent and useful techniques for dealing with such phenomena include the Khater approach [10] and the enhanced generalized Riccati mapping approach [11]. In this paper, a newly developed and more powerful technique, the generalized auxiliary equation mapping method is considered, which is a more generalized and robust version of the method proposed by Sirendaoreji [12], because the method provides an elegant way to reduce the computational complexity and helps in finding more generalized nature exact solutions [13].

The SNNV equation is important in stochastic partial differential equation (SPDE) theory. It helps study time dependence when randomness is present. Such equations model natural phenomena. The SPDEs generalize deterministic differential equations by adding time-dependent random fluctuations and have thus proved indispensable tools for system analysis under the influence of noise. The SNNV equation is widely used across scientific disciplines, including physics, biology, chemistry, geophysical dynamics, and climatology [14]. Compared to models in determinism, SPDEs include effects of stochastic influences on system behavior, hence having richer descriptions of time-evolving systems. The SNNV equation is found is widely used to describe wave dispersion, interactions between solitons, and stochastic effects on energy distribution. From modulating planar waves, offering general hyperbolic systems, and long-wave approximation solutions. Solving SPDEs exactly, however, remains challenging. The challenge has been overcome by several studies for several SPDEs, such as the mKdV equation [15], the Davey-Stewartson equation [16], and the Jimbo-Miwa equation [17]. We consider the stochastic Nizhnik-Novikov-Veselov

$$U_t + kU_{xxx} + rU_{yyy} + sU_x + qU_y - 3k(UV)x - 3r(UW)y + vU\beta_t = 0, \tag{1.1}$$

$$U_x = V_y, \qquad U_y = W_x, \tag{1.2}$$

here, v is the free control parameter, β_t is temporal noise (a Wiener process), and k, r, s, and q are free parameters. The SNNV system is an extension of the KdV equation and is observed in diverse physical systems, including sound waves in crystal lattices, ion-acoustic waves in plasmas, stably stratified ocean internal waves, shallow-water wave dynamics, and nonlinear optics. The solitary wave propagation in ideal conditions is governed by the SNNV equation in the classical case, but realistic wave interactions in natural systems require a richer description of multiple interacting waves. To address such complexities, we use the highly effective technique, EMAEM approach, to derive a soliton solution. This technique is computationally efficient, versatile across nonlinearities, and provides a precise solution. The versatility of the EMAEM technique makes it an invaluable resource, particularly for the study of stochastic phenomena in solitons.

Given its significance, researchers have attempted to obtain analytical solutions to the SNNV equation using various analytical tools, including the semi-inverse variational principle [18],

conservation law approach [19], tanh expansion approach [20], Lie symmetry analysis [21], modified simple equation approach [22], modified extended direct algebraic approach [23], and the Riccati approach [24]. Others include powerful methods such as the Adomian decomposition approach [25], the integrable nonlocal LPD equation approach [26]. A KMM system with variable coefficients in deformed ferrite is analyzed near a noncharacteristic movable singular manifold, yielding symbolic Magnetic Auto-Bäcklund Transformations and Magnetic Soliton Solutions [27]. A multivariate bilinear neural network is used to get more precise solutions for NLPDEs [28]. These have played vital roles in solving nonlinear partial differential equations (NLPDEs) found in scientific and engineering applications, and for which strong tools for accurate modeling are required [29].

A fundamental phenomenon in nonlinear dynamics is bifurcation, which exhibits transitions between stability and instability. Bifurcation analysis, originally developed by Liu and Li (2002) [30], is now an accepted methodology for analyzing soliton solutions in systems. Poincaré maps and phase diagrams, when applied, allow researchers to analyze chaotic behavior in nonlinear systems [31]. Bifurcation analysis is applied in our case to the SNNV equation via a solver, yielding novel solitary wave solutions that have not been reported before. To analyze chaotic behavior in greater detail, time series plots, Poincaré maps, and 2D and 3D phase diagrams, representing phase trajectories versus time through density and stream plots, are used. As an extension of wave models in nonlinear contexts in classical systems, SNNV is augmented by stochastic disturbances to replicate realistic systems under the influence of noise [32]. The SNNV equation has applications in several disciplines, including fluid flow, nonlinear optics, and plasma physics. The EMAEM approach is discovered to offer an excellent platform for extracting soliton solutions and their behavior under stochastic effects. The sensitivity of our system to initial conditions, a necessary property of chaotic behavior, is established in our presentation. We validate our results by performing a stability analysis using the Hamiltonian technique and systematically presenting them in an organized structure. Furthermore, for readers interested in recent trends related to nonlinear dynamics and Solitons, see [33–35].

Bifurcation analysis has become a pertinent tool for studying and discussing the behaviour of nonlinear dynamics, especially transitions between steady and unstable states. It is essential for studying bifurcation behaviors and soliton solutions in complex systems, and it was first identified by Liu and Li (2002) [30]. With the use of tools like phase diagrams and Poincarè maps, researchers can investigate chaotic features. By applying bifurcation analysis to the Stochastic Nizhnik-Novikov-Veselov equation of nonlinear nature using the unified solver technique mentioned, we visualized the chaotic behavior of the dynamical system and explores its various solitary wave solutions in the complex domain, which are not reported in the literature using other techniques. To identify and display the existence of chaos, time series diagrams, Poincarè maps, and 2D, 3D phase portraits, along with their tabular and image form, are used. Examples include plasma physics, nonlinear optics, and fluid mechanics. EMAEM analysis is an efficient technique for solving the given problem, allowing us to obtain the soliton solution and examine it when subjected to stochastic forcing. The sensitive dependence of the dynamical system on initial conditions has also been demonstrated. To verify the correctness of our calculations, we also performed a stability analysis of the obtained solitary wave solutions using the Hamiltonian technique in tabulated form.

The study focuses on understanding stochastic dynamical behavior in multidimensional nonlinear systems, where randomness significantly affects both soliton structures and stability. Contrary to previous proposed studies for deterministic models, we used the EMAEM. This is because EMAEM

has better capabilities for handling complex nonlinear equations, resulting in more precise results. The originality and novelty of the proposed study lie in discovering new forms of single, dark, and bright singular solitons for the SNNV equation, and in studying their characteristics regarding chaos, bifurcation, and stability.

The article is structured as follows: the SNNV is briefly reviewed in Section 1. Section 2 provides a detailed explanation of the methodology used in the suggested approach, based on the family of SNNV equations. In section 3, we look at the system dynamics stability analysis. Section 4 presents the chaotic behavior of system dynamics. The bifurcation analysis of the SNNV equation is explained in Section 5. Section 6 discusses the graphical representation of solutions. The SNNV equation's sensitivity analysis is looked at in Section 7. Section 8 presents the findings and comments. The closing remarks are included in Section 9.

2. Overview of EMAEM method

In this section, we concentrate on using the recently developed EMAEM method, presented by Seadawy and Cheema [36] and Pan et al. [37], to derive more novel and general travelling wave solutions for the SNNV system.

$$M(U, U_t, U_x, U_y, U_{xx}, U_{yy}, V_x, W_x, \beta_t \ldots) = 0. \tag{2.1}$$

In $M(x, y, t)$, where M is a polynomial, we apply the traveling wave transformation below to explicitly derive the exact travelling wave solution:

$$U(x, y, t) = R(X), \qquad X = \sum_{i=0}^{m} \nu_i x_i. \tag{2.2}$$

Equation (1.1) transforms into a nonlinear ODE of the following form using this transformation.

$$M_2(U, U', U'', U''', V', W' \ldots) = 0. \tag{2.3}$$

$$R(X) = \sum_{j=0}^{n} a_j F^j(X) + \sum_{j=-1}^{-n} b_{-j} F^j(X) + \sum_{j=2}^{n} c_j F^{j-2}(X) F'(X) + \sum_{j=1}^{n} d_j \left(\frac{F'(X)}{F(X)}\right)^j, \tag{2.4}$$

where the arbitrary constants a_j, b_j, c_j, and d_j must be determined. In this context, the following generalized solution is fulfilled by $F(X)$.

$$F'^2 = \left(\frac{dF}{dX}\right)^2 = \beta_1 F^2(X) + \beta_2 F^3(X) + \beta_3 F^4(X), \tag{2.5}$$

here $\beta_1, \beta_2, \beta_3$ will be found later.

The transformation is given by

$$U(x, y, t) = R(X) e^{(-\nu\beta(t) - \frac{\nu^2}{2}t)}, \; V(x, y, t) = S(X) e^{(-\nu\beta(t) - \frac{\nu^2}{2}t)}, \; W(x, y, t) = T(X) e^{(-\nu\beta(t) - \frac{\nu^2}{2}t)}, \tag{2.6}$$

$$X = lx + my - pt. \tag{2.7}$$

Adding Eqs (2.6) and (2.7) into Eq (1.1), we get stochastic ODEs, such

$$\left((kl^3 + rm^3)R''' + (sl + qm - p)R' - 3kl(RS)' - 3rm(RT)'\right)e^{(-v\beta(t)-\frac{v^2}{2}t)} = 0. \tag{2.8}$$

Now by assuming $(e^{(-v\beta(t)-\frac{v^2}{2}t)}) = 1$, we obtain,

$$(kl^3 + rm^3)R''' + (sl + qm - p)R' - 3kl(RS)' - 3rm(RT)' = 0, \tag{2.9}$$

$$lR' = mS', mR' = T'. \tag{2.10}$$

Integrating Eq (2.10), we obtain,

$$S = \frac{l}{m}R, T = \frac{m}{l}R. \tag{2.11}$$

Substituting Eq (2.11) into Eq (2.9), we have

$$(kl^3 + rm^3)R''' + (sl + qm - p)R' - 3(\frac{kl^2}{m} + \frac{rm^2}{l})(R^2)' = 0. \tag{2.12}$$

After integrating, we have

$$(kl^3 + rm^3)R'' + (sl + qm - p)R - 3(\frac{kl^2}{m} + \frac{rm^2}{l})R^2 = 0. \tag{2.13}$$

For the application of the balancing principle, we have

$$R'' + Q_1R - Q_2R^2 = 0, \tag{2.14}$$

where $Q_1 = \frac{sl+qm-p}{kl^3+rm^3}$, and $Q_2 = \frac{3}{ml}$.

Applying the balance principle yields $N = 2$. Therefore, Eq (2.4) simplifies as follows:

$$R(X) = a_0 + a_1F(X) + a_2F(X)^2 + \frac{b_1}{F(X)} + \frac{b_2}{F(X)^2} + c_2F'(X) + d_1\frac{F'(X)}{F(X)} + d_2\left(\frac{F'(X)}{F(X)}\right)^2, \tag{2.15}$$

where a_0, a_1, a_2, b_1, b_2, c_2, d_1, and d_2 are constants to be determined.

Family 1:

$$a_0 = \frac{1}{3}f(lm-3),\ \ a_1 = \frac{1}{2}g(lm-2),\ \ a_2 = h(lm-1),\ \ c_2 = \sqrt{h}lm,\ \ b_1 = b_2 = d_1 = 0,\ \ d_2 = 1. \tag{2.16}$$

$$r_1(x,y,t) = \frac{1}{12}e^{\left(-\frac{tv^2}{2}-\beta tv\right)}f\left(\frac{3A^4j^2}{B^2} - \frac{6A^2\sqrt{f}\sqrt{h}jlm}{g} + 4(-3+lm) - 6(-2+lm)B + \frac{12fh(-1+lmB^2)}{g^2}\right),$$

where

$$X = lx + my - pt, A = \operatorname{sech}\left(\frac{1}{2}\sqrt{f}(X+X_0)\right), B = 1 + j\tanh\left(\frac{1}{2}\sqrt{f}(X+X_0)\right).$$

$$r_2(x,y,t) = e^{\left(-\frac{tv^2}{2}-\beta tv\right)}\left(\frac{1}{2}F\sqrt{h}lm\sqrt{\frac{f}{h}} + \frac{1}{4}Eg\sqrt{\frac{f}{h}}(lm-2) + \frac{1}{3}f(lm-3) + \frac{1}{4}E^2f(lm-1) + \frac{F^2}{E^2}\right),$$

where

$$X = lx + my - pt, E = \left(\frac{j \sinh\left(\sqrt{f}\,(X + X_0)\right)}{\cosh\left(\sqrt{f}\,(X + X_0)\right) + \rho} + 1 \right),$$

$$F = \left(\frac{\sqrt{f} j \cosh\left(\sqrt{f}\,(X + X_0)\right)}{\cosh\left(\sqrt{f}\,(X + X_0)\right) + \rho} - \frac{\sqrt{f} j \sinh^2\left(\sqrt{f}\,(X + X_0)\right)}{\left(\cosh\left(\sqrt{f}\,(X + X_0)\right) + \rho\right)^2} \right).$$

$$r_3(x,y,t) = e^{\left(-\frac{tv^2}{2} - \beta tv\right)} \left(\frac{f^{3/2}\sqrt{h} jlm(-H\sigma + IG)}{g(H+\sigma)^2} + \frac{f j^2(-H\sigma + IG)^2}{J^2(H+\sigma)^4} + \frac{1}{3} f(lm-3) + \frac{f^2 h J^2(lm-1)}{g^2} - \frac{1}{2} fJ(lm-2) \right),$$

where

$$X = lx + my - pt, G = \cosh\left(\sqrt{f}\,(X + X_0)\right), H = \sinh\left(\sqrt{f}\,(X + X_0)\right), I = \rho\sqrt{\sigma^2 + 1} + 1, J = 1 + \frac{(G+I)j}{H+\sigma}.$$

Family 2:

$$a_0 = \frac{-6fk - 6fr - p + q + s}{6(k+r)},\ a_1 = a_2 = c_2 = b_1 = b_2 = 0,\ d_1 = \frac{i(p-q-s)}{\sqrt{-36fk^2 - 72fkr - 36fr^2}},\ d_2 = i. \tag{2.17}$$

$$r_4(x,y,t) = e^{\left(-\frac{tv^2}{2} - \beta tv\right)} \left(L + M \frac{\operatorname{sech}^2\left(\frac{1}{2}\sqrt{f}\,(X + X_0)\right)}{j \tanh\left(\frac{1}{2}\sqrt{f}\,(X + X_0)\right) + 1} + \frac{if j^2 \operatorname{sech}^4\left(\frac{1}{2}\sqrt{f}\,(X + X_0)\right)}{4\left(j \tanh\left(\frac{1}{2}\sqrt{f}\,(X + X_0)\right) + 1\right)^2} \right),$$

where

$$X = lx + my - pt, L = \frac{-6fk - 6fr - p + q + s}{6(k+r)}, M = \frac{i\sqrt{f} j(p-q-s)}{2\sqrt{-36fk^2 - 72fkr - 36fr^2}}.$$

$$r_5(x,y,t) = e^{\left(-\frac{tv^2}{2} - \beta tv\right)} \left(\frac{iF(p-q-s)}{E\sqrt{-36fk^2 - 72fkr - 36fr^2}} + \frac{-6fk - 6fr - p + q + s}{6(k+r)} + \frac{iF^2}{E^2} \right),$$

where

$$X = lx + my - pt, E = \left(\frac{j \sinh\left(\sqrt{f}\,(X + X_0)\right)}{\cosh\left(\sqrt{f}\,(X + X_0)\right) + \rho} + 1 \right),$$

$$F = \left(\frac{\sqrt{f} j \cosh\left(\sqrt{f}\,(X + X_0)\right)}{\cosh\left(\sqrt{f}\,(X + X_0)\right) + \rho} - \frac{\sqrt{f} j \sinh^2\left(\sqrt{f}\,(X + X_0)\right)}{\left(\cosh\left(\sqrt{f}\,(X + X_0)\right) + \rho\right)^2} \right).$$

$$r_6(x,y,t) = e^{\left(-\frac{tv^2}{2} - \beta tv\right)} \left(\frac{-6fk - p + q - 6fr + s}{6(k+r)} + \frac{if j^2(IG - \sigma H)^2}{(\sigma + H)^2 J^2} - \frac{i\sqrt{f} j(p-q-s)(IG - \sigma H)}{(\sigma+H)^2 J\sqrt{-36fk^2 - 72fkr - 36fr^2}} \right),$$

where

$$X = lx + my - pt,\ G = \cosh\left(\sqrt{f}\,(X + X_0)\right),\ H = \sinh\left(\sqrt{f}\,(X + X_0)\right),\ I = \rho\sqrt{\sigma^2 + 1} + 1,\ J = 1 + \frac{(G+I)j}{H+\sigma}.$$

Family 3:

$$a_1 = \frac{3g - fglm}{3f},\ a_2 = \frac{3h - fhlm}{3f},\ c_2 = b_1 = b_2 = d_1 = 0,\ d_2 = \frac{flm - 3}{3f},\ a_0 = 1. \tag{2.18}$$

$$r_7(x,y,t)=\frac{1}{12}e^{\left(-\frac{tv^2}{2}-\beta tv\right)}\left(\frac{A^4j^2(flm-3)}{B^2}-\frac{4B^2fh(flm-3)}{g^2}+4B(flm-3)+12\right),$$

where

$$X=lx+my-pt, A=\operatorname{sech}\left(\frac{1}{2}\sqrt{f}\,(X+X_0)\right), B=1+j\tanh\left(\frac{1}{2}\sqrt{f}\,(X+X_0)\right).$$

$$r_8(x,y,t)=e^{\left(-\frac{tv^2}{2}-\beta tv\right)}\left(\frac{F^2(flm-3)}{3E^2f}+\frac{E\sqrt{\frac{f}{h}}(3g-fglm)}{6f}+\frac{E^2(3h-fhlm)}{12h}+1\right),$$

where

$$X=lx+my-pt, E=\left(\frac{j\sinh\left(\sqrt{f}\,(X+X_0)\right)}{\cosh\left(\sqrt{f}\,(X+X_0)\right)+\rho}+1\right),$$

$$F=\left(\frac{\sqrt{f}\,j\cosh\left(\sqrt{f}\,(X+X_0)\right)}{\cosh\left(\sqrt{f}\,(X+X_0)\right)+\rho}-\frac{\sqrt{f}\,j\sinh^2\left(\sqrt{f}\,(X+X_0)\right)}{\left(\cosh\left(\sqrt{f}\,(X+X_0)\right)+\rho\right)^2}\right).$$

$$r_9(x,y,t)=e^{\left(-\frac{tv^2}{2}-\beta tv\right)}\left(\frac{fJ^2(3h-fhlm)}{3g^2}-\frac{J(3g-fglm)}{3g}+\frac{j^2(flm-3)(-H\sigma+IG)^2}{3J^2(H+\sigma)^4}+1\right),$$

where

$$X=lx+my-pt,\ G=\cosh\left(\sqrt{f}\,(X+X_0)\right),\ H=\sinh\left(\sqrt{f}\,(X+X_0)\right),\ I=\rho\sqrt{\sigma^2+1}+1,\ J=1+\frac{(G+I)j}{H+\sigma}.$$

Family 4:

$$a_1=\frac{g\left(3kl^3-l^2ms-lm^2q+lmp+3m^3r\right)}{3f\left(kl^3+m^3r\right)},\ \ a_2=c_2=b_1=b_2=d_1=0,$$
$$d_2=\frac{-3kl^3+l^2ms+lm^2q-lmp-3m^3r}{3f\left(kl^3+m^3r\right)},\ \ a_0=1. \tag{2.19}$$

$$r_{10}(x,y,t)=e^{\left(-\frac{tv^2}{2}-\beta tv\right)}\left(1-\frac{Dj^2\operatorname{sech}^4\left(\frac{1}{2}\sqrt{f}\,(X+X_0)\right)}{12\left(j\tanh\left(\frac{1}{2}\sqrt{f}\,(X+X_0)\right)+1\right)^2}-\frac{1}{3}D\left(j\tanh\left(\frac{1}{2}\sqrt{f}\,(X+X_0)\right)+1\right)\right),$$

where

$$X=lx+my-pt, D=\frac{3kl^3-l^2ms+lm(p-mq)+3m^3r}{kl^3+m^3r}.$$

$$r_{11}(x,y,t)=e^{\left(-\frac{tv^2}{2}-\beta tv\right)}\left(\frac{(-C)F^2}{3E^2f\left(kl^3+m^3r\right)}+\frac{ECg\sqrt{\frac{f}{h}}}{6f\left(kl^3+m^3r\right)}+1\right),$$

where

$$X=lx+my-pt, E=\left(\frac{j\sinh\left(\sqrt{f}\,(X+X_0)\right)}{\cosh\left(\sqrt{f}\,(X+X_0)\right)+\rho}+1\right),$$

$$F = \left(\frac{\sqrt{f}\, j \cosh\left(\sqrt{f}\,(X+X_0)\right)}{\cosh\left(\sqrt{f}\,(X+X_0)\right)+\rho} - \frac{\sqrt{f}\, j \sinh^2\left(\sqrt{f}\,(X+X_0)\right)}{\left(\cosh\left(\sqrt{f}\,(X+X_0)\right)+\rho\right)^2} \right),$$

$$C = \left(3kl^3 - l^2ms + lm(p-mq) + 3m^3r\right).$$

$$r_{12}(x,y,t) = e^{\left(-\frac{tv^2}{2}-\beta tv\right)}\left(-\frac{Cj^2(\mathrm{IG}-H\sigma)^2}{3J^2(H+\sigma)^4\left(kl^3+m^3r\right)} - \frac{CJ}{3\left(kl^3+m^3r\right)} + 1 \right),$$

where

$$X = lx + my - pt, G = \cosh\left(\sqrt{f}\,(X+X_0)\right), H = \sinh\left(\sqrt{f}\,(X+X_0)\right),$$

$$I = \rho\sqrt{\sigma^2+1}+1, J = 1 + \frac{(G+I)j}{H+\sigma}, C = \left(3kl^3 - l^2ms + lm(p-mq) + 3m^3r\right).$$

3. Stability analysis

The stability of the traveling wave solutions for Eq (2.14) is analyzed using the Hamiltonian method, as detailed below:

$$U = \int_{-\infty}^{\infty} \frac{R(x)^2}{2} dx, \tag{3.1}$$

where D indicates the Hamiltonian-system (HS) momentum and $R(x)$ is a traveling wave solution. This is the definition of the necessary stability criterion:

$$\frac{\partial D}{\partial v} > 0. \tag{3.2}$$

The wave velocity is represented by v. We use Eqs (3.1) and (3.2) to identify parameters and ranges where the traveling wave solutions of the HS are stable. Using the necessary stability conditions in these respective ranges, we derive the following stability features of our solutions. A detailed classification of all derived solutions along with their stability behavior is provided in Table 1.

Table 1. Stability Analysis of $r_i(x,y,t)$ $1 \le i \le 12$.

No.	*Solution*	*Stability*	*Values of the variables*
1	$r_1(x,y,t)$	*Stable*	$f = 2.3, g = 1.5, j = -1.4, X_0 = -1.6, m = 2.7, v = 1, -1 \le x,t \le 1$
2	$r_2(x,y,t)$	*Stable*	$h = -1.1, j = -1.4, v = 3, X_0 = 1.2, p = -2.8, y = 1.9, -4 \le x,t \le 4$
3	$r_3(x,y,t)$	*Stable*	$m = 2.5, v = 2, j = 1, y = 1.5, X_0 = 3.3, h = -4, \rho = -3.2, -3 \le x,t \le 3$
4	$r_4(x,y,t)$	*Stable*	$l = -1.5, v = 5, f = 1.3, j = -1.4, y = -1.9, h = -1.3, k = -1.1, -6 \le x,t \le 6$
5	$r_5(x,y,t)$	*Unstable*	*Singular solution*
6	$r_6(x,y,t)$	*Stable*	$l = 1.7, m = 2, v = 4, f = -0.9, q = -3.2\ y = 0.9, X_0 = -1.3, -5 \le x,t \le 5$
7	$r_7(x,y,t)$	*Stable*	$f = 3, g = 2.2, v = 5, h = 2.3, j = -3.4, l = -2.5, m = -2.7\ -7 \le x,t \le 7$
8	$r_8(x,y,t)$	*Stable*	$l = 0.2, m = 3.8, v = 6, j = -3.5, y = -1.3, X_0 = -2.3, -8 \le x,t \le 8$
9	$r_9(x,y,t)$	*Unstable*	*Singular solution*
10	$r_{10}(x,y,t)$	*Stable*	$j = -1.4, y = 3.9, v = 8, X_0 = -1.6, k = -3.1, g = 1.2, s = 2.4, -9 \le x,t \le 9$
11	$r_{11}(x,y,t)$	*Unstable*	*Singular solution*
12	$r_{12}(x,y,t)$	*Stable*	$j = -5, y = -2.5, v = 6, X_0 = -1.3, \rho = 1.2, \beta = -2.4, -10 \le x,t \le 10$

4. Chaotic behavior with phase portrait

In this section, we discuss the quasi-periodic chaotic behaviour. The planar dynamical equation's perturbation term is

$$\frac{dR}{dX} = \omega, \tag{4.1}$$

$$\frac{d\omega}{dX} = -Q_1 R + Q_2 R^2 + N(X), \tag{4.2}$$

where $N(X) = \alpha \sin(\beta X), \alpha \cos(\beta X), \alpha \cosh(\beta X)$ and $(Ae^{-0.02X})$. The two parameters in perturbation terms are α and β. The amplitude and frequency of an external force applied to a planar dynamical system are represented by parameters α and β, respectively. The impact of these perturbation terms on the previously indicated structure Eqs (4.1) and (4.2) is now evaluated. The governing model's chaotic behavior is observed when suitable parameter, frequency, and intensity values are considered, as shown in Figures 1–4. Time series representations of chaotic nature, Poincarè sections, and 2D and 3D phase portraits are provided.

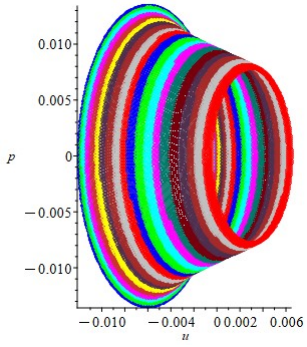

(a) 2D Phase portraits of chaotic behavior of dynamical Eqs (4.1) and (4.2) when a trigonometric function cos is considered a perturbation term.

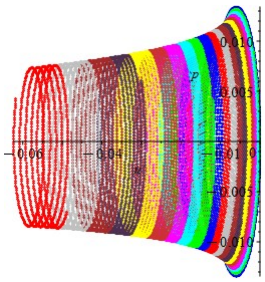

(b) 2D Phase portraits of chaotic behavior of dynamical Eqs (4.1) and (4.2) when a trigonometric function cosh is considered a perturbation term.

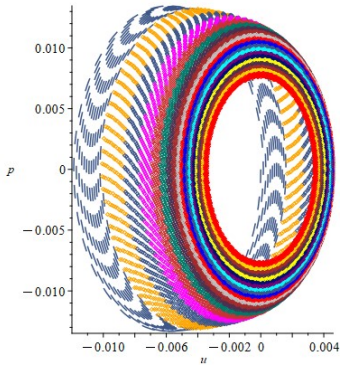

(c) 2D Phase portraits of chaotic behavior of dynamical Eqs (4.1) and (4.2) when a trigonometric function exp is considered a perturbation term.

Figure 1. Graphic representation of 2D phase portraits of Eqs (4.1) and (4.2) with different values of $N(X) = \alpha \cos(\beta X)$, $\alpha \cosh(\beta X)$ *and* $\alpha \exp(\beta X)$ with $\alpha = -0.03$.

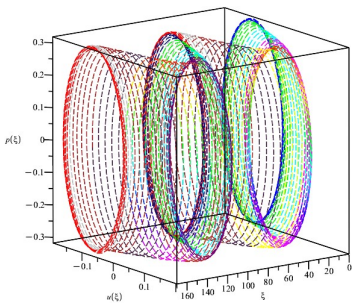

(a) 3D Phase portraits of chaotic behavior of dynamical Eqs (4.1) and (4.2) when a trigonometric function cos is considered a perturbation term.

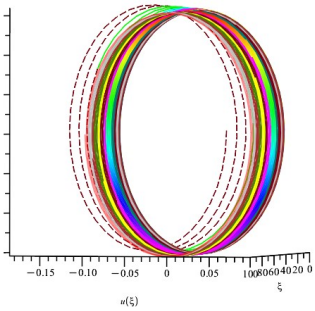

(b) 3D Phase portraits of chaotic behavior of dynamical Eqs (4.1) and (4.2) when a trigonometric function exp is considered a perturbation term.

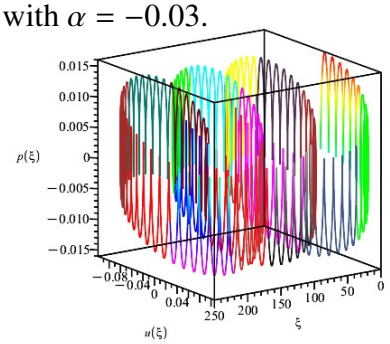

(c) 3D Phase portraits of chaotic behavior of dynamical Eqs (4.1) and (4.2) when a trigonometric function sin is considered a perturbation term.

Figure 2. Graphic representation of 3D phase portraits of Eqs (4.1) and (4.2) with different values of $N(X) = \alpha \cos(\beta X)$, $\alpha \exp(\beta X)$ *and* $\alpha \sin(\beta X)$ with $\alpha = -1$.

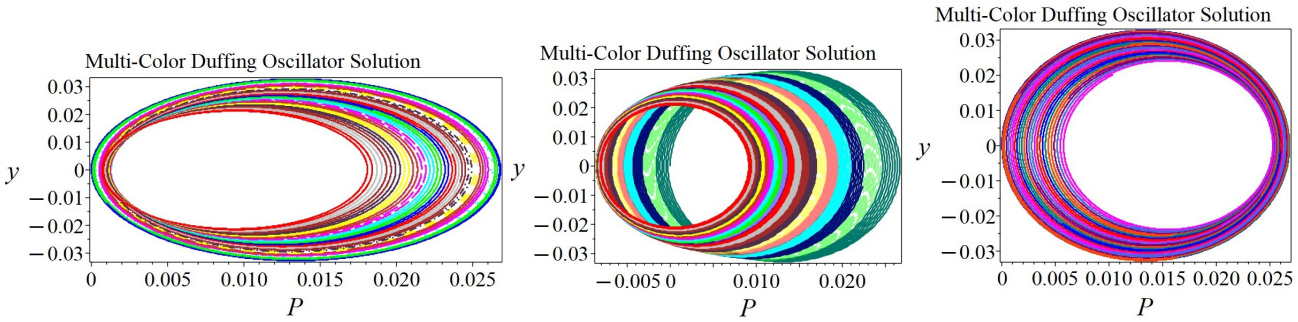

(a) Poincare Phase cos (b) Poincare Phase exp (c) Poincare Phase cosh

Figure 3. Graphic representation of 3D phase portraits of Eqs (4.1) and (4.2) with different values of $N(X) = \alpha\cos(\beta X)$, $\alpha\exp(\beta X)$ *and* $\alpha\cosh(\beta X)$ with $\alpha = 0.08$.

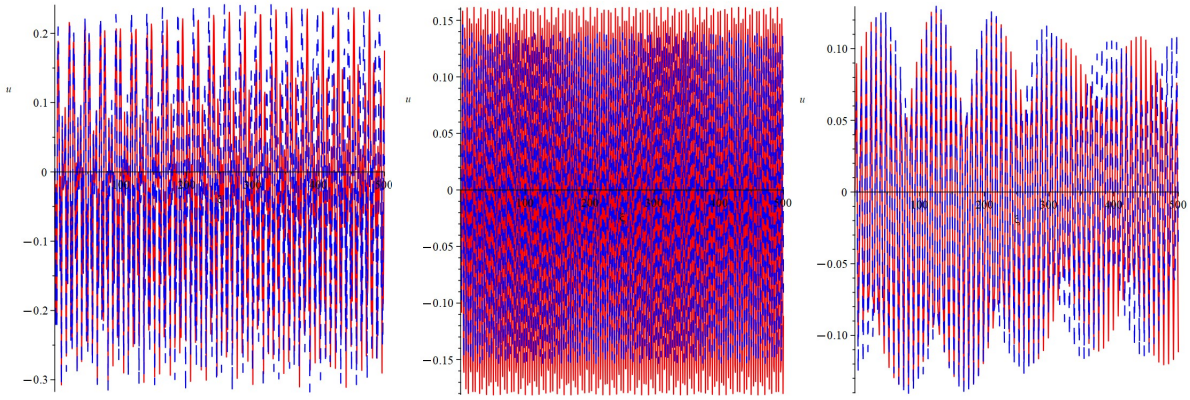

(a) Time series Phase sin (b) Time series Phase exp (c) Time series Phase cos

Figure 4. Graphic representation of 3D phase portraits of Eqs (4.1) and (4.2) with different values of $N(X) = \alpha\sin(\beta X)$, $\alpha\exp(\beta X)$ *and* $\alpha\cos(\beta X)$, *whereas* $A = 70 and B = -70$.

5. Bifurcation analysis

The term "bifurcation" refers to the mathematical changes that occur within a system and affect the kind of solutions the differential equations yield. The mathematical structure of dynamic systems is frequently examined using it. When a system's behavior suddenly shifts due to a slight alteration in its parameter values, this is known as a bifurcation. By addressing local and global aspects of one-dimensional operator separation in Banach spaces, this concept demonstrates how split equality issues can be resolved using the theory. The specific arrangement of bifurcating solutions and common structural features, such as stability, are also investigated. Through the application of the Galilean transformation, it is possible to convert Eq (2.14) into two systems of equations. Next, using the Hamiltonian function, Eq (2.14) is transformed into the dynamical form shown below:

$$\frac{dR}{dX} = \omega, \tag{5.1}$$

$$\frac{d\omega}{dX} = -Q_1 R + Q_2 R^2, \tag{5.2}$$

$$H(R,\omega) = \frac{1}{2}\omega^2 - \frac{Q_1}{2}R^2 + \frac{Q_2}{3}R^3 = h, \tag{5.3}$$

where $Q_1 = \frac{sl+qm-p}{kl^3+rm^3}$, $Q_2 = \frac{3}{ml}$ and h is referred to as Hamiltonian Constant.

Furthermore, h, is total energy, $\frac{1}{2}\omega^2$ is kinetic energy and $-\frac{Q_1}{2}R^2 + \frac{Q_2}{3}R^3$ is the potential energy. For finding the equilibrium points of system Eq (5.2), the solution for this system is inevitable:

$$\omega = 0, \tag{5.4}$$

$$-Q_1R + Q_2R^2 = 0. \tag{5.5}$$

We get two equilibrium points: $R_1 = (0,0)$, $R_2 = \left(\frac{Q_1}{Q_2}\right)$.

Jacobian matrix determinant of Eqs (5.1) and (5.2).

$$J = \begin{vmatrix} 0 & 1 \\ -Q_1R + Q_2R^2 & 0 \end{vmatrix},$$

$$J(R,\omega) = -(-Q_1R + Q_2R^2). \tag{5.6}$$

The following claims, which are founded on ideas of planar dynamics, are true: (R,ω) is a saddle point (R,ω) if $J(R,\omega) < 0$. For $J(R,\omega) > 0$, the center point is at (R,ω). The cuspidal point is at (R,ω) when $J(R,\omega) = 0$. Here, we adjust the relevant parameter values to illustrate the potential outcomes and to illustrate the qualitative behavior of the system under different parameter conditions, the phase portraits are presented in Figure 5:

Case 1. $Q_1 > 0, Q_2 > 0$.
Case 2. $Q_1 > 0, Q_2 < 0$.
Case 3. $Q_1 < 0, Q_2 < 0$.
Case 4. $Q_1 < 0, Q_2 > 0$.

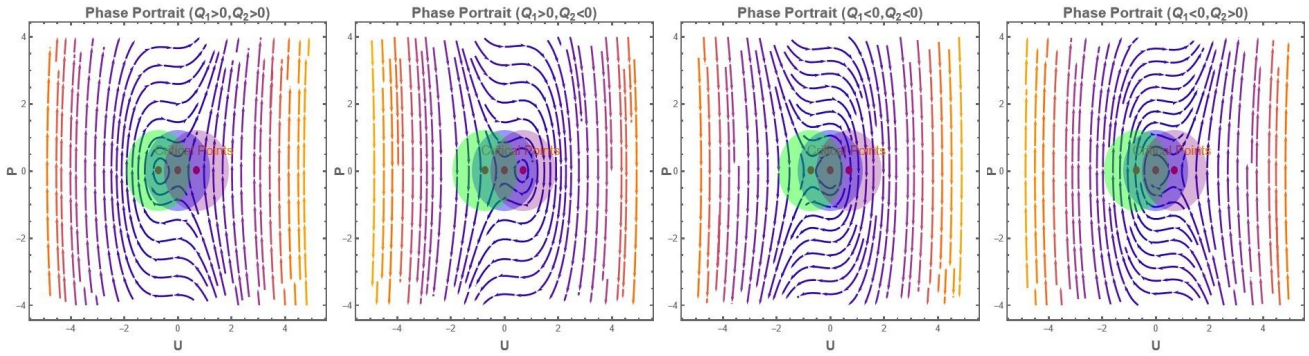

(a) Phase Portrait Q_1>0, Q_2>0 (b) Phase Portrait Q_1>0, Q_2<0 (c) Phase Portrait Q_1<0, Q_2<0 (d) Phase Portrait Q_1<0, Q_2>0

Figure 5. Graphical representation of Phase portraits within the dynamic framework of Eqs (5.1) and (5.2)

6. Analytical graphical representation

Using Mathematica 13.3 and Maple, we present graphical representations of our discovered solutions in several dimensions (rational, trigonometric, mixed, and hyperbolic functions in various

forms). The objective is to gain a better understanding of the physical architecture of fractional shallow-water wave occurrences. The plots display different kinds of solitons from traveling wave solutions. Figures 6 to 10 are mostly bright solitons with localized peak-shaped waves that decay smoothly to zero, as evident from the plots in 3D, contour, and density. The profiles are sharp-peaked for a few, showing singular bright solitons. The wave profiles in Figure 11 are localized dips against a non-zero background, making them anti-dark solitons. The figures collectively display bright, singular bright, and anti-dark solitons, characterized by their amplitude localization and wave behavior.

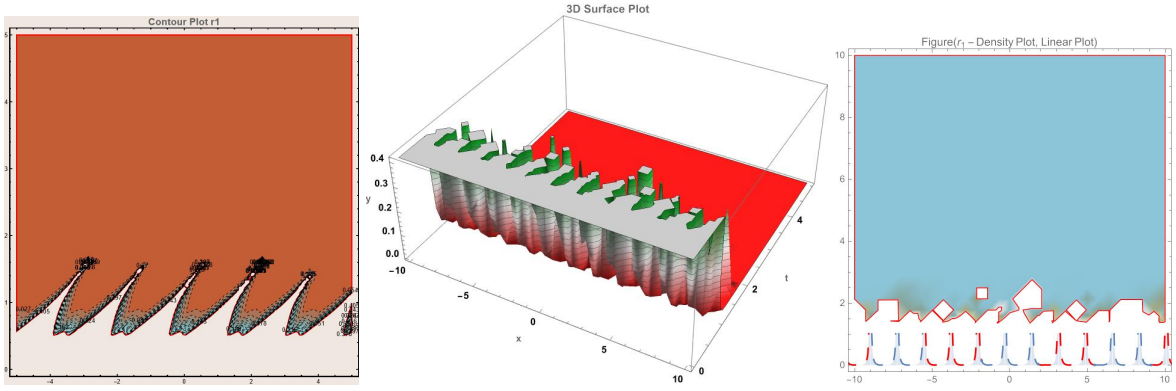

(a) Contour Plot of r_1 (b) 3D surface Plot of r_1 (c) Density linear Plot of r_1

Figure 6. Graphical visualization of traveling wave for $r_1(x, y, t)$ with Parameters $f = -2.1$, $g = -3.2$, $h = -4.3$, $j = -3.4$, $l = -2.5$, $X_0 = -1.6$, $m = -2.7$. (a) The Contour Profile of traveling wave with intervals (-5,5), (0,5). (b) 3D Surface Profile of traveling wave with intervals (-10,10), (0,5). (c) Density linear Profile of traveling wave with intervals (-10,10), (0,10).

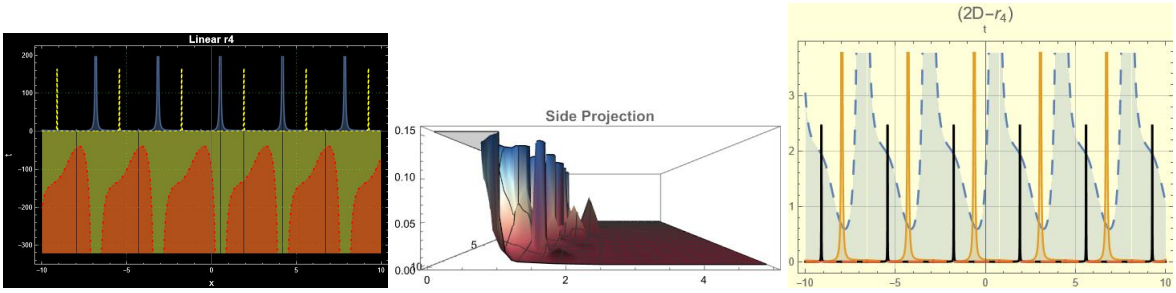

(a) Linear Plot of r_4 (b) Side-Projection of r_4 (c) 2D Plot of r_4

Figure 7. Graphical visualization of traveling wave for $r_4(x, y, t)$ with Parameters $m = -2.7$, $p = -3.8$, $y = -1.9$, $v = -2$, $\beta = -1.1$, $k = -2.6$. (a) The Linear Profile of traveling wave with intervals (-10,10), (0,3). (b) Side-Projection Profile of traveling wave with intervals (-10,10), (0,5). (c) 2D Profile of travelling wave with interval (-10,10).

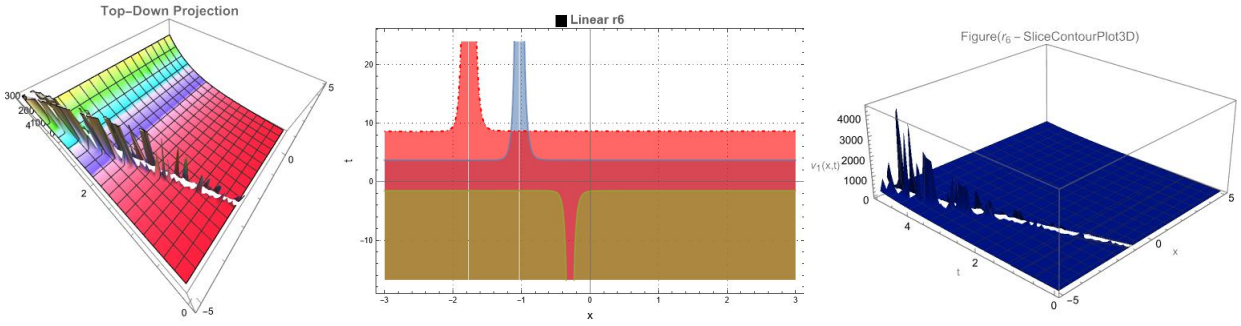

(a) Top-Down Projection of r_6 (b) Linear Plot of r_6 (c) 3D Slice Contour of r_6

Figure 8. Graphical visualization of travelling wave for $r_6(x, y, t)$ with Parameters $l = 2.7$, $m = 1.5$, $f = 3.8$, $j = 3$, $y = 1.5$, $X_0 = 1.3$, $h = -1$. (a) The Top-Down Projection Profile of traveling wave with intervals (-5,5), (0,5). (b) Linear Profile of traveling wave with interval (-5,5). (c) 3D Slice Contour Profile of traveling wave with intervals (-5,5), (0,5).

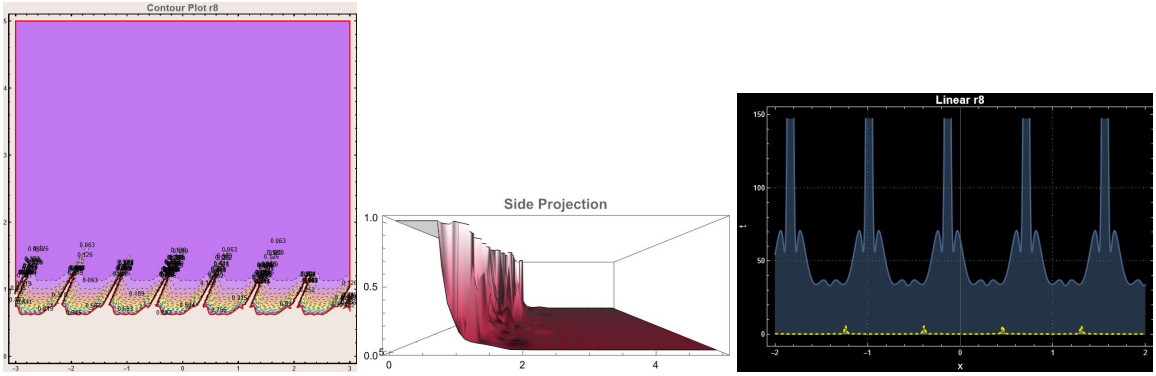

(a) Contour Plot of r_8 (b) Side Projection of r_8 (c) Linear Plot of r_8

Figure 9. Graphical visualization of traveling wave for $r_8(x, y, t)$ with Parameters $l = -3.7$, $m = -3.8$, $f = -4$, $j = -3.5$, $y = -1.3$, $X_0 = -2.3$, $h = -3$. (a) The Contour Profile of traveling wave with intervals (-5,5), (0,3). (b) Side Projection of traveling wave with intervals (-5,5), (0,5). (c) Linear Profile of traveling wave with interval (-2,2).

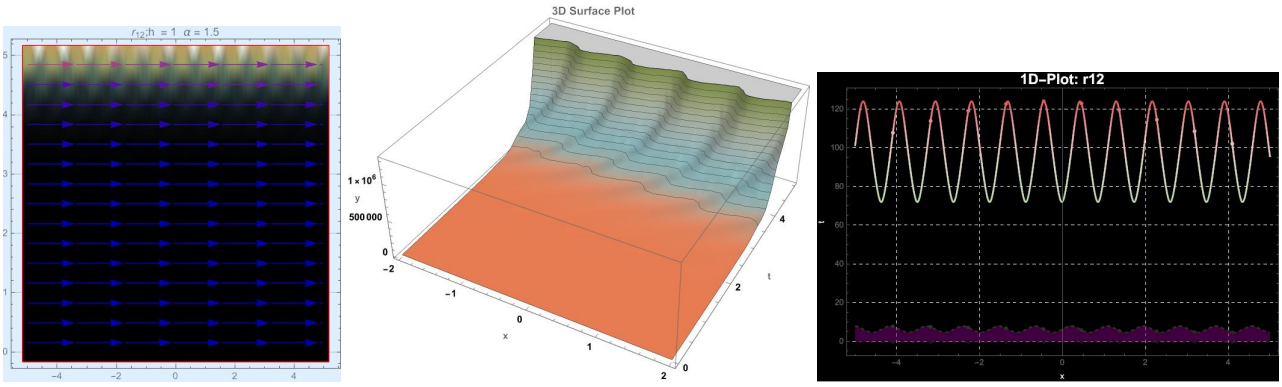

(a) Steam Density Plot of r_{12} (b) 3D-Surface Plot of r_{12} (c) 1D-Plot of r_{12}

Figure 10. Graphical visualization of travelling wave for $r_{12}(x, y, t)$ with Parameters $f = -3.8$, $j = 5$, $y = -2.5$, $X_0 = 1.3$, $p = -4$, $\rho = 1.2$, $\beta = -2.4$. (a) The Steam Density Profile of traveling wave with intervals (-5,5), (0,5). (b) 3D-Surface Profile of traveling wave with interval (-5,5). (c) 1D Profile of traveling wave with intervals (-2,2), (0,5).

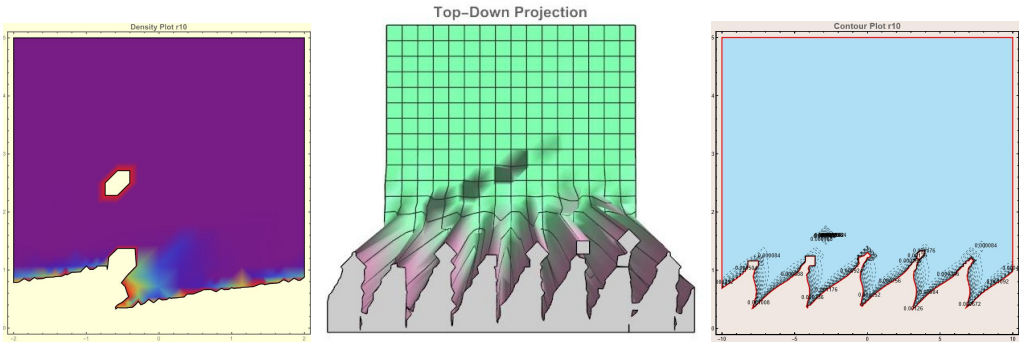

(a) Density Plot of r_{10} (b) Top-Down Projection Plot of r_{10} (c) Contour Plot of r_{10}

Figure 11. Graphical visualization of traveling wave for $r_{10}(x, y, t)$ with Parameters $f = -1.3$, $g = -1.2$, $j = -1.4$, $l = -1.5$, $X_0 = -1.6$. (a) The Density Profile of traveling wave with intervals (-2,2), (0,5). (b) Top-Down Projection Profile of travelling wave with intervals (-15,15), (0,3). (c) Contour Profile of traveling wave with intervals (-10,10), (0,5).

7. Sensitivity

The graphical representations of the dynamical system's sensitivity to initial conditions in different dimensions for Eqs (4.1) and (4.2) have been presented in this section. A sensitivity analysis of the dynamical system is thus performed using initial conditions. Given $R^{'} = \omega(X)$, Eq (2.14) can be transformed using the Galilean transformation to become:

$$\frac{dR}{dX} = \omega(X), \tag{7.1}$$

$$\frac{d\omega}{dX} = -Q_1 R(X) + Q_2 R(X)^2. \tag{7.2}$$

A comprehensive graphical analysis of the system's dynamics is provided in Figures 12–17, where the trajectories and wave profiles corresponding to different initial conditions are compared side by side. These figures clearly demonstrate the system's sensitivity to initial data, with noticeable differences in oscillatory patterns and peak structures. Such visualizations complement the theoretical results and emphasize the role of initial circumstances in shaping the overall evolution of the solutions.

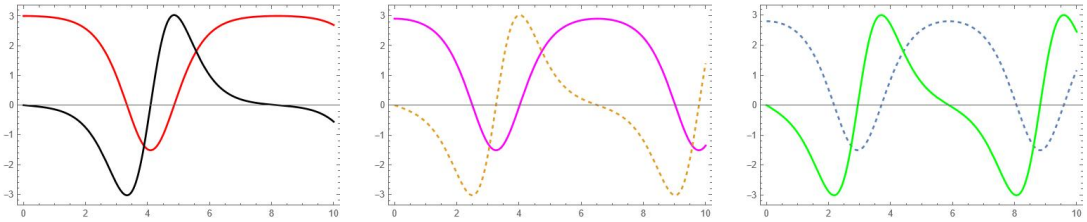

(a) Two curves with initial condition $(R, \omega) = (3, 0)$ (b) Two curves with initial condition $(R, \omega) = (2.9, 0)$ (c) Two curves with initial condition $(R, \omega) = (2.8, 0)$

Figure 12. The system governed by Eqs (7.1) and (7.2) is shown in sensitivity analysis for different initial circumstances. In portion (a), the numerical solution for $(R(0), \omega(0)) = (3, 0)$ is displayed. Over the time span $[0, 10]$, the black curve represents $\omega(X)$ while the red curve represents $R(X)$. While part (c) shows the solution for $(R(0), \omega(0)) = (2.8, 0)$, part (b) shows the system's reaction for the initial condition $(R(0), \omega(0)) = (2.9, 0)$. The sensitivity of the dynamical system to slight variations in the initial circumstances is evident from these figures.

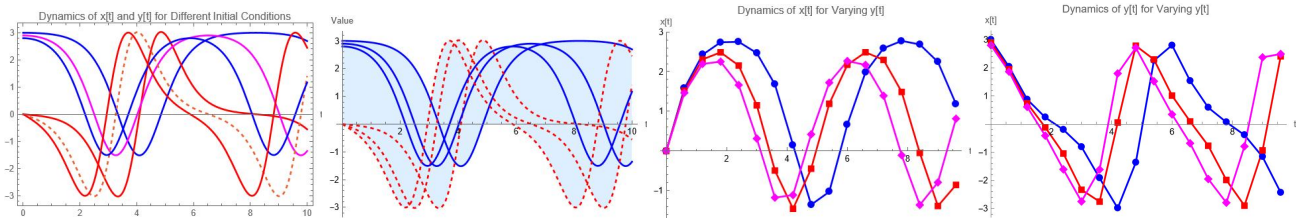

(a) Sensitive dependence over different Initial Conditions together

(b) V wave Pattern R(0) and waves $\omega(0)$ with shaded regions

(c) List Plot of $R(0)$ with varying $\omega(0) = (3, 2.9, 2, 8)$

(d) List Plot of $\omega(0)$ with varying $\omega(0) = (3, 2.9, 2.8)$

Figure 13. Three distinct initial conditions are used to present sensitivity analysis of the dynamical system. Trajectories for $(R(X), \omega(X)) = (3, 0), (2.9, 0), (2.8, 0)$ are displayed in parts (a) and (b), with the shaded areas amply demonstrating the system's sensitivity to variations in the initial circumstances. Wave profiles of $R(X)$ for fixed $R(0) = 0$ and variable $\omega(0) = 3, 2.9, 2.8$ are shown in part (c), which forms a clear V-pattern. The impact of initial conditions on system dynamics across the time interval $[0, 10]$ is highlighted in part (d), which displays the corresponding wave profiles of $\omega(X)$ for the same set of initial values.

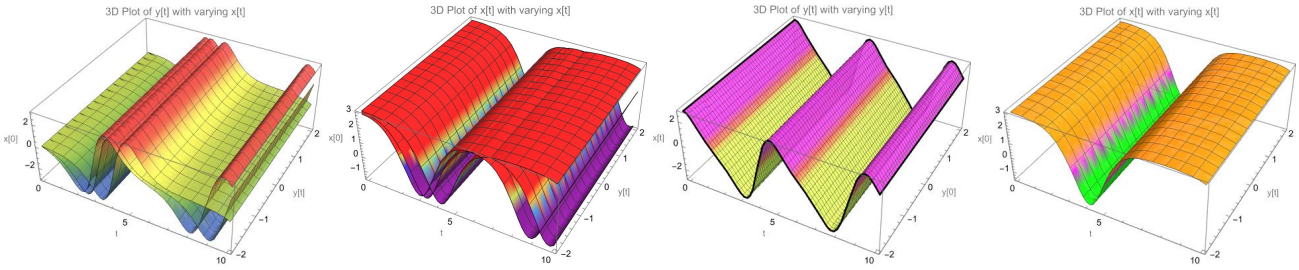

(a) 3D Plot of $\omega(X)$ with varying $R(0) = (3, 2.9, 2.8)$

(b) 3D Plot of $R(X)$ with varying $R(0) = (3, 2.9, 2.8)$

(c) 3D Plot $\omega(X)$ which show w wave pattern with varying $(R(X), \omega(X)) = (0, 2.8)$

(d) 3D Plot of $R(X)$ which show v wave pattern with varying $(R(X), \omega(X)) = (3, 0)$

Figure 14. The 3D plots of $R(X)$ and $\omega(X)$ are depicted in the pictures, demonstrating how they change dynamically under different beginning conditions. $R(X)$ and $\omega(X)$ exhibit general evolution patterns in parts (a) and (b), respectively. Part (d) shows a V-shaped wave profile of $R(X)$ for the initial condition $(R(X), \omega(X)) = (3, 0)$, part (c) shows a W-shaped wave profile for the starting condition $(R(X), \omega(X)) = (0, 2.8)$. As time passes, the system's delicate reliance on initial conditions is made evident by these visualizations.

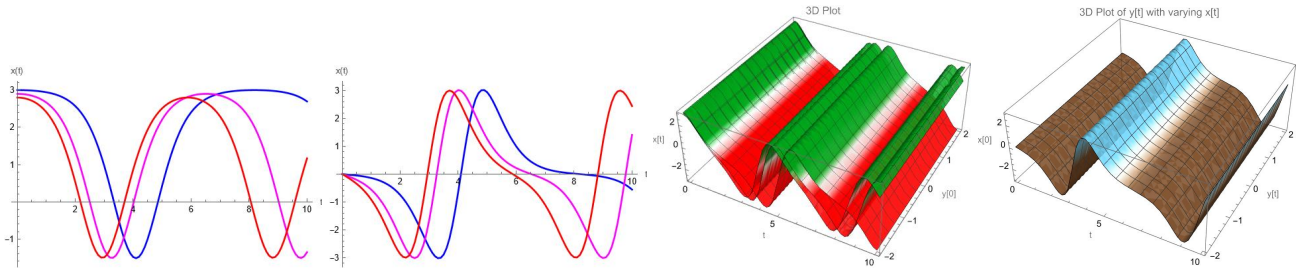

(a) 2D Plot of $R(0)$ with varying $R(0) = (3, 2.9, 2.8)$ (b) 2D Plot of $\omega(0)$ with varying $R(0) = (3, 2.9, 2.8)$ (c) 3D Plot of $\omega(0)$ with varying $\omega(0) = (3, 2.9, 2.8)$ (d) 3D Plot of $\omega(0)$ with varying $(R(0), 0) = (2.8, 0)$

Figure 15. The dynamical system's sensitivity analysis under initial conditions is shown in the figure. With $\omega(0) = 0$, the numerical solutions of $R(X)$ for $R(0) = 3,\ 2.9,\ 2.8$ are displayed in part (a). Periodic wave profiles are revealed by the matching solutions of $\omega(X)$ in Part (b). In Part (c), the behavior of $\omega(X)$ with fixed $R(0) = 0$ and various beginning conditions $\omega(0) = 3,\ 2.9,\ 2.8$ is demonstrated, along with periodic patterns. The wave profile of $\omega(X)$ for the fixed initial condition $(R(0), \omega(0)) = (2.8, 0)$ is shown in part (d). Plotting the system's sensitive dependence on beginning circumstances over the time span $[0, 10]$ together shows that even little changes in $R(0)$ can have a big impact on how the system evolves.

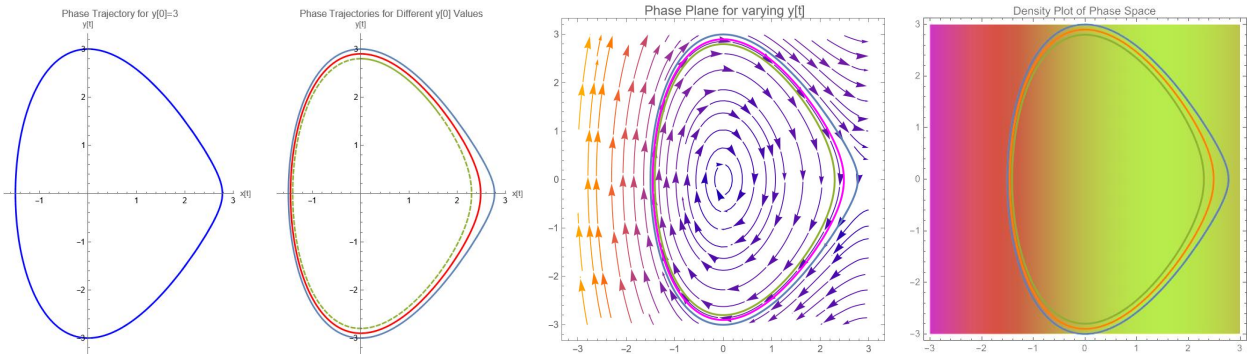

(a) Phase Trajectories for $\omega(0) = (3)$ value (b) Phase Trajectories for different $\omega(0)=(3, 2.9, 2.8)$ values (c) Phase Plane for varying $\omega(0)=(3, 2.9, 2.8)$ (d) Density Plot of Phase Space

Figure 16. The phase trajectory of the dynamical system is shown in part (a). $(R(0), \omega(0)) = (0, 3)$ as the initial condition for (7.1) and (7.2). Phase trajectories for various initial conditions $\omega(0) = 3,\ 2.9,\ 2.8$ with fixed $R(0) = 0$ are shown in Part (b). The accompanying phase plane charts, which depict the system's evolution under these beginning conditions, are displayed in Part (c). The density plot of the phase space over time for the identical initial conditions is shown in Part (d), which illustrates how sensitive the system is to slight changes in $\omega(0)$ with $R(0) = 0$.

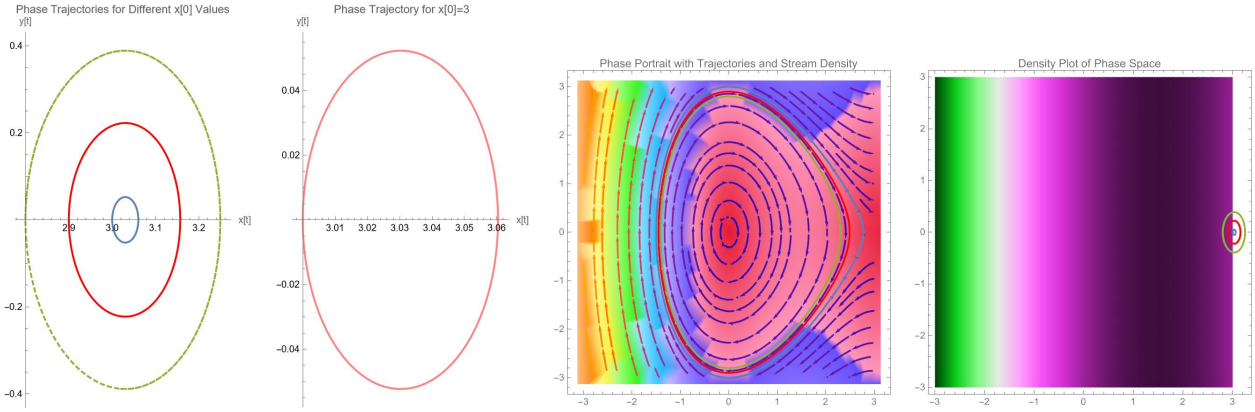

(a) Phase Trajectories for different $R(0) = (3, 2.9, 2.8)$ values

(b) Phase Trajectories for $R(0) = (3)$ value

(c) Phase Portrait with Trajectories and Stream Density

(d) Density Plot of Phase Space

Figure 17. The dynamical system's phase trajectories are displayed in Part (a). (7.1) and (7.2) in the opening circumstances with $R(0) = 0$ fixed, $\omega(0) = 3, 2.9, 2.8$. The phase trajectory for the single beginning condition is shown in part (b). $(0, 3) = (R(0), \omega(0))$. The phase portrait for various beginning conditions is shown in Part (c), which includes both trajectories and stream density. $R(0) = 0$ and $\omega(0) = 3, 2.9, 2.8$. The density map of the phase space over time for initial conditions is shown in Part (d). $\omega(0) = 0$ and $R(0) = 3, 2.9, 2.8$. The system's sensitivity to beginning conditions is demonstrated by these visualizations taken together.

8. Discussion

In this section, we discuss the comparisons and differences between the discovered families from results and those previously documented in the literature. Various standard analytic approaches to the SNNV system are considered.

- First, our proposed method for constructing new families of results in Eq (2.4) has a unique structure that is novel and distinct, given a combination of three parameters. The largest and most obvious difference is this.
- Second, we employ several sets of constant values a_j, b_j, c_j, and d_j to graphically depict the dynamics of our obtained results in multiple dimensions using mathematical tools such as Mathematica 13.3 and Maple.
- Equation (2.4) provides many new and practical analytical solutions, like combination functions, functions of rational type, functions of trigonometric type, and hyperbolic functions. Observing this is imperative.

The Solutions found by the Sardar subequation method, Modified generalized rational exponential function method, Jacobi elliptic function method, Burgers' equation, Extended tanh-function method, Truncated Mittag-Leffler function, tanh-coth method, sine-cosine method, and the Modified Simplest Equation method were all discussed and found to differ significantly from our latest presented solutions. These dissimilarities were observed in comparison with the findings presented in [38–40],

respectively.

9. Conclusions

The generalized form of the traditional SNNV equation, which incorporates stochastic disturbances, is known as the SNNV system. It can model noisy processes in fields like fluid dynamics, nonlinear optics, and plasma physics. Our objectives of the study will be to obtain exact soliton solutions for the equation presented and to investigate the stochastic process characteristics of the solutions using the EMAEM. The applicability and flexibility of the EMAEM approach for solving complex nonlinear equations were demonstrated through various solitons generated by the equation, including isolated, bright, and dark solitons. A comprehensive analysis was also carried out for the generalized SNNV system. This system describes the propagation of optical pulses through nonlinear media. The corresponding planar dynamical system was obtained using the Galilean transformation. Its analysis is performed via bifurcation analysis. An external forcing system was used to study the possibility of chaos in the system. This is examined using two-, three-, and four-dimensional phase portraits and time series analysis.

The Hamiltonian technique was used for stability analysis of the solitary wave solutions. The obtained results are documented in tables for accuracy. Sensitivity and modulation instability analyses were presented for different initial conditions. These indicated that the system is stable, as small variations in initial conditions lead to insignificant changes in the solution. Mathematica software was used to produce 2D, 3D, and contour plots to graphically present the solutions. The results are presented as pathwise (sample path) solutions to the SNNV equation, depicting the deterministic process each stochastic process follows along a given noise path. The introduction strengthens the conceptual interpretation of the stochastic framework adopted for the study.

Future work in this direction could focus on developing stochastic models and their soliton solutions using Lie symmetry and neural network approaches.

Author contributions

Hafiz M. A. Siddiqui: Supervision, Data Curation, Methodology; Lotfi Jlali: Project Administration, Visualization; A. Nazir: Investigation, Writing-Original Draft, Software; Syed T. R. Rizvi: Writing-Review Editing, Formal Analysis; Atef F. Hashem: Conceptualization, Resources, Software; Aly R. Seadawy: Validation, Project Administration, Resources, Data Curation.

Use of Generative-AI tools declaration

The authors declare they have not used Artificial Intelligence (AI) tools in the creation of this article.

Funding

This work was supported and funded by the Deanship of Scientific Research at Imam Mohammad Ibn Saud Islamic University (IMSIU) (grant number IMSIU-DDRSP2502).

Conflict of interest

The authors declare no conflict of interest.

References

1. W. Malfliet, Solitary wave solutions of nonlinear wave equations, *Am. J. Phys.*, **60** (1992), 650–654. https://doi.org/10.1119/1.17120
2. E. Zahran, M. Khater, Modified extended tanh-function method and its applications to the Bogoyavlenskii equation, *Appl. Math. Model.*, **40** (2016), 1769–1775. https://doi.org/10.1016/j.apm.2015.08.018
3. F. Xie, J. Chen, Z. Lü, Using symbolic computation to exactly solve the integrable Broer-Kaup equations in (2+1)-dimensional spaces, *Commun. Theor. Phys.*, **43** (2005), 585. https://doi.org/10.1088/0253-6102/43/4/003
4. I. Inan, Y. Ugurlu, H. Bulut, Auto-Bäcklund transformation for some nonlinear partial differential equation, *Optik*, **127** (2016), 10780–10785. https://doi.org/10.1016/j.ijleo.2016.08.115
5. H. Hu, X. Jia, B. Sang, Painlevé analysis and symmetry group for the coupled Zakharov-Kuznetsov equation, *Phys. Lett. A*, **375** (2011), 3459–3463. https://doi.org/10.1016/j.physleta.2011.07.058
6. D. Kumar, R. Agarwal, J. Singh, A modified numerical scheme and convergence analysis for fractional model of Liénard's equation, *J. Comput. Appl. Math.*, **339** (2018), 405–413. https://doi.org/10.1016/j.cam.2017.03.011
7. N. Kudryashov, One method for finding exact solutions of nonlinear differential equations, *Commun. Nonlinear Sci.*, **17** (2012), 2248–2253. https://doi.org/10.1016/j.cnsns.2011.10.016
8. M. Kaplan, A. Bekir, A. Akbulut, A generalized Kudryashov method to some nonlinear evolution equations in mathematical physics, *Nonlinear Dyn.*, **85** (2016), 2843–2850. https://doi.org/10.1007/s11071-016-2867-1
9. A. Bekir, M. Kaplan, Exponential rational function method for solving nonlinear equations arising in various physical models, *Chinese J. Phys.*, **54** (2016), 365–370. https://doi.org/10.1016/j.cjph.2016.04.020
10. S. Naqvi, I. Aldawish, S. Rizvi, A. Seadawy, Bilinear neural network solutions for nonlinear waves in the Sawada-Kotera model studied in heat transfer, *Eur. Phys. J. Plus*, **140** (2025), 835. https://doi.org/10.1140/epjp/s13360-025-06781-4
11. N. Cheemaa, H. Siddiqui, B. Nazir, A. Bekir, A. Almehizia, H. Hussein, Stability, sensitivity, chaotic behavior, and phase trajectories evaluation of the Davey-Stewartson stochastic equation, *Nonlinear Dyn.*, **113** (2025), 17209–17225. https://doi.org/10.1007/s11071-025-10912-y
12. Sirendaoreji, Auxiliary equation method and new solutions of Klein-Gordon equations, *Chaos Soliton. Fract.*, **31** (2007), 943–950. https://doi.org/10.1016/j.chaos.2005.10.048
13. N. Cheemaa, A. Seadawy, H. Rezazadeh, Bright-dark solitary wave solutions of coupled integrable (2+1)-dimensional Maccari system in applied physics, *New Trends in Physical Science Research*, **1** (2022), 31–45. https://doi.org/10.9734/bpi/ntpsr/v1/1969B
14. L. Arnold, Random dynamical systems, In: *Dynamical systems*, Berlin: Springer, 2006, 1–43. https://doi.org/10.1007/BFb0095238

15. W. Mohammed, F. Al-Askar, C. Cesarano, The analytical solutions of the stochastic mKdV equation via the mapping method, *Mathematics*, **10** (2022), 4212. https://doi.org/10.3390/math10224212
16. F. Al-Askar, C. Cesarano, W. Mohammed, Multiplicative Brownian motion stabilizes the exact stochastic solutions of the Davey-Stewartson equations, *Symmetry*, **14** (2022), 2176. https://doi.org/10.3390/sym14102176
17. F. Al-Askar, C. Cesarano, W. Mohammed, The solitary solutions for the stochastic Jimbo-Miwa equation perturbed by white noise, *Symmetry*, **15** (2023), 1153. https://doi.org/10.3390/sym15061153
18. R. Alqahtani, M. Babatin, A. Biswas, Bright optical solitons for Lakshmanan-Porsezian-Daniel model by semi-inverse variational principle, *Optik*, **154** (2018), 109–114. https://doi.org/10.1016/j.ijleo.2017.09.112
19. A. Biswas, A. Kara, R. Alqahtani, M. Ullah, H. Triki, M. Belic, Conservation laws for optical solitons of Lakshmanan-Porsezian-Daniel model, *Proc. Romanian Acad. A*, **19** (2018), 39–44.
20. J. Manafian, M. Foroutan, A. Guzali, Applications of the ETEM for obtaining optical soliton solutions for the Lakshmanan-Porsezian-Daniel model, *Eur. Phys. J. Plus*, **132** (2017), 494. https://doi.org/10.1140/epjp/i2017-11762-7
21. A. Biswas, Theory of optical couplers, *Opt. Quant. Electron.*, **35** (2003), 221–235. https://doi.org/10.1023/A:1022852801087
22. A. Biswas, M. Ekici, A. Sonmezoglu, H. Triki, F. Majid, Q. Zhou, et al., Optical solitons with Lakshmanan-Porsezian-Daniel model using a couple of integration schemes, *Optik*, **158** (2018), 705–711. https://doi.org/10.1016/j.ijleo.2017.12.190
23. M. Hubert, G. Betchewe, M. Justin, S. Doka, K. Crepin, A. Biswas, et al., Optical solitons with Lakshmanan-Porsezian-Daniel model by modified extended direct algebraic method, *Optik*, **162** (2018), 228–236. https://doi.org/10.1016/j.ijleo.2018.02.091
24. A. Al Qarni, A. Ebaid, A. Alshaery, H. Bakodah, A. Biswas, S. Khan, et al., Optical solitons for Lakshmanan-Porsezian-Daniel model by Riccati equation approach, *Optik*, **182** (2019), 922–929. https://doi.org/10.1016/j.ijleo.2019.01.057
25. A. Al Qarni, M. Banaja, H. Bakodah, A. Alshaery, Q. Zhou, A. Biswas, et al., Bright optical solitons for Lakshmanan-Porsezian-Daniel model with spatio-temporal dispersion by improved Adomian decomposition method, *Optik*, **181** (2019), 891–897. https://doi.org/10.1016/j.ijleo.2018.12.172
26. W. Liu, D. Qiu, Z. Wu, J. He, Dynamical behavior of solution in integrable nonlocal Lakshmanan-Porsezian-Daniel equation, *Commun. Theor. Phys.*, **65** (2016), 671. https://doi.org/10.1088/0253-6102/65/6/671
27. X. Gao, J. Liu, G. Wang, Inhomogeneity, magnetic auto-Bäcklund transformations and magnetic solitons for a generalized variable-coefficient Kraenkel-Manna-Merle system in a deformed ferrite, *Appl. Math. Lett.*, **171** (2025), 109615. https://doi.org/10.1016/j.aml.2025.109615
28. J. Liu, W. Zhu, Y. Wu, G. Jin, Application of multivariate bilinear neural network method to fractional partial differential equations, *Results Phys.*, **47** (2023), 106341. https://doi.org/10.1016/j.rinp.2023.106341

29. S. Ahmed, I. Aldawish, S. Rizvi, A. Seadawy, Iterative investigation of the nonlinear fractional Cahn-Allen and fractional clannish random walker's parabolic equations by using the hybrid decomposition method, *Fractal Fract.*, **9** (2025), 656. https://doi.org/10.3390/fractalfract9100656
30. Z. Liu, J. Li, Bifurcations of solitary waves and domain wall waves for KdV-like equation with higher-order nonlinearity, *Int. J. Bifurcat. Chaos*, **12** (2002), 397–407. https://doi.org/10.1142/S0218127402004425
31. A. Seadawy, A. Ali, T. Radwan, W. Mohammed, K. Ahmed, Solitary wave solutions for the conformable time-fractional coupled Konno-Oono model via applications of three mathematical methods, *AIMS Mathematics*, **10** (2025), 16027–16044. https://doi.org/10.3934/math.2025718
32. S. Rizvi, I. Alazman, Nimra, A. Seadawy, Elliptic functions and advanced analysis of soliton solutions for the Dullin-Gottwald-Holm dynamical equation with applications of mathematical methods, *Symmetry*, **17** (2025), 1773. https://doi.org/10.3390/sym17101773
33. J. Yu, F. Yu, L. Li, Soliton solutions and strange wave solutions for (2+1)-dimensional nonlocal nonlinear Schrödinger equation with PT-symmetric term, *Appl. Math. Lett.*, **168** (2025), 109583. https://doi.org/10.1016/j.aml.2025.109583
34. L. Li, F. Yu, Some mixed soliton wave interaction patterns and stabilities for Rabi-coupled nonlocal Gross-Pitaevskii equations, *Chaos Soliton. Fract.*, **194** (2025), 116171. https://doi.org/10.1016/j.chaos.2025.116171
35. Q. Qin, L. Li, F. Yu, Dark matter-wave bound soliton molecules and modulation stability for spin-1 Gross-Pitaevskii equations in Bose-Einstein condensates, *Chaos Soliton. Fract.*, **196** (2025), 116365. https://doi.org/10.1016/j.chaos.2025.116365
36. A. Seadawy, N. Cheemaa, Applications of extended modified auxiliary equation mapping method for high-order dispersive extended nonlinear Schrödinger equation in nonlinear optics, *Mod. Phys. Lett. B*, **33** (2019), 1950203. https://doi.org/10.1142/S0217984919502038
37. C. Pan, N. Cheemaa, W. Lin, M. Inc, Nonlinear fiber optics with water wave flumes: dynamics of the optical solitons of the derivative nonlinear Schrödinger equation, *Opt. Quant. Electron.*, **56** (2024), 434. https://doi.org/10.1007/s11082-023-05985-1
38. H. Rehman, R. Akber, A. Wazwaz, H. Alshehri, M. Osman, Analysis of Brownian motion in stochastic Schrödinger wave equation using Sardar sub-equation method, *Optik*, **289** (2023), 171305. https://doi.org/10.1016/j.ijleo.2023.171305
39. J. Ahmad, Z. Mustafa, S. Rehman, N. Turki, N. Shah, Solitary wave structures for the stochastic Nizhnik-Novikov-Veselov system via modified generalized rational exponential function method, *Results Phys.*, **52** (2023), 106776. https://doi.org/10.1016/j.rinp.2023.106776
40. A. Wazwaz, The sine-cosine method for obtaining solutions with compact and noncompact structures, *Appl. Math. Comput.*, **159** (2004), 559–576. https://doi.org/10.1016/j.amc.2003.08.136

AIMS Press